Temperature effects on RNA polymerase initiation kinetics reveal which open complex initiates and that bubble collapse is stepwise

Dylan M. Plaskon[a,1], Kate L. Henderson[a,1], Lindsey C. Felth[a], Cristen M. Molzahn[a], Claire Evensen[a], Sarah Dyke[a], Irina A. Shkel[a,b], and M. Thomas Record Jr[a,b,2]

[a]Department of Biochemistry, University of Wisconsin–Madison, Madison, WI 53706; and [b]Department of Chemistry, University of Wisconsin–Madison, Madison, WI 53706

Edited by Peter H. von Hippel, University of Oregon, Eugene, OR, and approved May 19, 2021 (received for review October 21, 2020)

Transcription initiation is highly regulated by promoter sequence, transcription factors, and ligands. All known transcription inhibitors, an important class of antibiotics, act in initiation. To understand regulation and inhibition, the biophysical mechanisms of formation and stabilization of the "open" promoter complex (OC), of synthesis of a short RNA–DNA hybrid upon nucleotide addition, and of escape of RNA polymerase (RNAP) from the promoter must be understood. We previously found that RNAP forms three different OC with λP_R promoter DNA. The 37 °C RNAP-λP_R OC (RP_O) is very stable. At lower temperatures, RP_O is less stable and in equilibrium with an intermediate OC (I_3). Here, we report step-by-step rapid quench-flow kinetic data for initiation and growth of the RNA–DNA hybrid at 25 and 37 °C that yield rate constants for each step of productive nucleotide addition. Analyzed together, with previously published data at 19 °C, our results reveal that I_3 and not RP_O is the productive initiation complex at all temperatures. From the strong variations of rate constants and activation energies and entropies for individual steps of hybrid extension, we deduce that contacts of RNAP with the bubble strands are disrupted stepwise as the hybrid grows and translocates. Stepwise disruption of RNAP-strand contacts is accompanied by stepwise bubble collapse, base stacking, and duplex formation, as the hybrid extends to a 9-mer prior to disruption of upstream DNA–RNAP contacts and escape of RNAP from the promoter.

transcription | initiation | regulation | thermodynamics | kinetics

Transcription of DNA information into RNA is fundamental to all life. In prokaryotes, all transcription is performed by a single multisubunit RNA polymerase (RNAP). Gene expression is highly regulated, and much of this regulation occurs in the steps of transcription initiation. Promoter sequences, transcription factors, ligands, and conditions are key regulatory variables (1–3). All known transcription inhibitors, an important class of antibiotics, act in initiation (4). Fig. 1*A* shows the sequence and the key regions of λP_R-promoter DNA. These include the -35 and -10 hexamers, the 6 bp discriminator region between the -10 region and the transcription start site (TSS, +1), and the initial transcribed region (ITR).

Stages of productive initiation are summarized in Fig. 1*B*. Specific binding of RNAP to duplex (closed) promoter DNA forms an ensemble of closed complexes (CC), including an initial closed intermediate (designated RP_C) and a series of more advanced closed intermediates (collectively called I_1), in which the promoter DNA is remodeled. "Isomerization" of the ensemble of CC intermediates, including the opening of the DNA from the −10 region to the TSS, forms a series of open complexes (OC), including an initial unstable open intermediate (I_2), which at λP_R promoter converts to more stable species (intermediate I_3, stable 37 °C complex RP_O), all with the same open region but with different interactions involving the discriminator strands and the ITR (for representations of these OC, see Fig. 1*C*). Nucleotide triphosphates (NTPs) complementary to the template DNA sequence are bound and the corresponding monophosphates (NMP) incorporated into an RNA–DNA hybrid in a series of initial transcription complexes (ITCs). The hybrid translocates into the cleft with each step of RNA extension, stressing and disrupting RNAP-promoter contacts so that RNAP escapes from the promoter in the transition from initiation to elongation.

Initiation in all likelihood is regulated at all of these stages. To understand regulation, the detailed mechanisms of these stages must be understood. Recent structural (5–9), kinetic–mechanistic (10–19), and high-throughput sequencing studies (20, 21) have greatly advanced our understanding of initiation, but much remains to be learned for the rational discovery of drug targets and for the design of synthetic promoters optimized for specific applications in molecular biology and medical biotechnology (22).

Many examples exist of the regulation of initiation at the CC level (i.e., rates and extents of CC formation and isomerization) by promoter sequences, factors, ligands, and conditions (2–4). Regulation of initiation at the OC level is potentially also significant but not at all well understood. Correlations of OC stability or lifetime with TSS selection (23), promoter output (24), and RNA–DNA hybrid length for RNAP escape have been proposed (15). The three λP_R OC in Fig. 1*C* differ in lifetime and stability by four orders of magnitude (lifetimes ranging from ∼1 s (I_2) to ∼13 h (RP_O) at 37 °C) (11, 15, 25). The question of which OC is/are

Significance

To transcribe DNA sequences into RNA, RNA polymerase (RNAP) first binds to promoter DNA. The promoter sequence dictates both binding strength and rate of remodeling the DNA duplex by RNAP to open 13 base pairs in the start site region. This open "bubble" allows complementary nucleotides to pair with template-strand bases and be incorporated into RNA. All sequence-specific, RNAP-promoter contacts must break for RNAP to escape and elongate the RNA, but how this occurs is not well understood. Here, we report rate constants for each initiation step at the λPR promoter at different temperatures. We analyze these data to obtain insights into which open complex initiates and when RNAP-promoter contacts are disrupted, allowing bubble collapse, duplex formation, and promoter escape.

Author contributions: K.L.H. and M.T.R. designed research; K.L.H., L.C.F., C.M.M., C.E., S.D., and M.T.R. performed research; D.M.P., K.L.H., I.A.S., and M.T.R. analyzed data; and D.M.P., K.L.H., and M.T.R. wrote the paper.

The authors declare no competing interest.

This article is a PNAS Direct Submission.

[1]D.M.P. and K.L.H. contributed equally to this work.

[2]To whom correspondence may be addressed. Email: mtrecord@wisc.edu.

This article contains supporting information online at https://www.pnas.org/lookup/suppl/doi:10.1073/pnas.2021941118/-/DCSupplemental.

Published July 21, 2021.

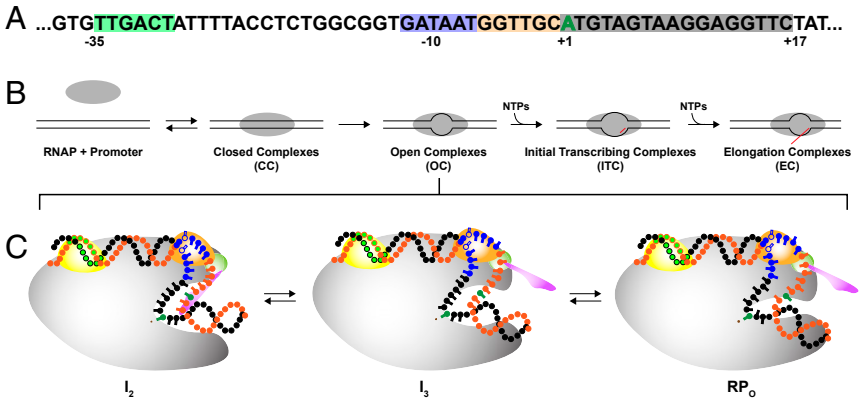

Fig. 1. Transcription initiation at λP_R promoter. (*A*) Nontemplate strand sequence of the λP_R promoter studied here, in which the ITR is modified to eliminate the incorporation of CMP before position +17, so transcription halts at a 16-mer RNA when CTP is withheld. The −35 (green), −10 (blue), and discriminator (tan) elements and the start site (+1; green) and ITR (gray) are highlighted. (*B*) Summary of stages in productive initiation by RNAP holoenzyme ($\alpha_2\beta\beta'\omega\sigma^{70}$). Key aspects of the mechanisms of two of these stages (OC and ITC) are determined in this study. (*C*) Schematic representation of OC species at the λP_R promoter at 37 °C: intermediates I_2 and I_3 and stable 37 °C complex RP_O. As illustrated, interactions of in-cleft and downstream elements of RNAP with the discriminator and ITR, weak or absent in I_2, are stronger in I_3 and much stronger in RP_O at 37 °C (10). RNAP core (gray) is shown with relevant σ^{70} subunits 1.1 (purple), 1.2 (green), 2 (light orange), and 4 (yellow). Linking domains between subunits are not shown for clarity. The template DNA strand is shown in black and the nontemplate strand in orange, with the −35 (light green), −10 (blue), and start site (dark green) indicated.

capable of productive initiation in the presence of NTPs has not been addressed previously for any promoter. As shown schematically in Fig. 1*C*, the λP_R OC differ in the strength of in-cleft interactions with the discriminator strands and of interactions of the downstream duplex (ITR) with downstream mobile elements (DMEs) of RNAP (11, 26–28). The difference in stability between RP_O and I_3 is known to decrease at temperatures below 37 °C, but otherwise, I_3 is much less characterized than RP_O and I_2. Formation equilibrium constants and lifetimes of OC at the well-studied T7A1 and *rrnB* P1 promoters are ∼1 and 3 orders of magnitude less than for λP_R. These OCs are proposed to be similar in their downstream interactions to λP_R I_3 and I_2, respectively (11).

For the transition from initiation to elongation to occur, specific RNAP-promoter contacts (29) must be disrupted by translocation of the RNA–DNA hybrid into the upstream cleft (6, 16, 30–34). Disruption of these RNAP-promoter contacts results in the collapse of (and duplex formation by) the upstream portion of the initiation bubble (−1 to −11 for λP_R), escape of RNAP from the promoter, and dissociation of the σ^{70} subunit (12, 35). Escape of RNAP from the λP_R promoter occurs after synthesis of an initial 10-mer RNA (15, 35).

To investigate these processes in the escape of RNAP, we previously determined the step-by-step kinetics and mechanism of NMP incorporation into the growing RNA–DNA hybrid at the λP_R promoter at 19 °C up to the escape point (16). This information, not available for any other promoter DNA or multisubunit RNAP, parallels that obtained for the single-subunit T7 bacteriophage RNAP (36). From an analysis of the repeated pattern of small and larger rate constants found for successive steps of RNA extension in initial transcription, we proposed that disruption of RNAP-promoter contacts occur in a stepwise manner prior to promoter escape (16).

Here, we report the 25 and 37 °C kinetics of initial transcription at the λP_R promoter. Rapid quench mixing is used to determine overall rates of full-length (FL) RNA synthesis and rate constants for the individual steps of NMP incorporation into the RNA–DNA hybrid at two NTP conditions for comparison with 19 °C results. A change in the initial step of the mechanism at 37 °C, as compared to 19 °C, reveals that the stable 37 °C OC (RP_O) cannot initiate and that an intermediate in RP_O formation (I_3) is the initiation complex. From analysis of the temperature dependence of these rate constants, we deduce when specific contacts of RNAP with single-stranded (ss) and duplex regions of promoter DNA are disrupted as the hybrid translocates into the cleft, resulting in the collapse of the initiation bubble, duplex formation, and escape of RNAP from the promoter.

Results

Unexpected Effects of Temperature on the Rate of Transcription Initiation at the λP_R Promoter. Time courses spanning more than two orders of magnitude (≤0.5 to ≥90 s) of transcription initiation by *Escherichia coli* RNAP at the λP_R promoter at 37 and 25 °C were obtained by rapid mixing at two different sets of NTP concentrations (designated "low UTP" and "high UTP") for comparison with previous results at 19 °C (16). The initial transcribed sequence (Fig. 1*A*), specifying a RNA that starts with pppApU, is modified from that of λP_R to eliminate the need for CTP until position +17, causing RNA synthesis by productive complexes to pause after 16-mer production when CTP is omitted. The competitor heparin, added with the NTP mixture, ensures single-round productive initiation by preventing reinitiation by any dissociated RNAP.

Fig. 2 *A* and *B* show representative polyacrylamide gel electrophoresis (PAGE) separations of RNAs present in samples quenched at a series of time points during initiation and the transition to elongation at the low-UTP condition (final concentrations 10 μM UTP, 200 μM ATP and GTP (no CTP), and 17.5 nM α-^{32}P-UTP) at 25 and 37 °C. *SI Appendix*, Fig. S1 shows representative gels from initiation kinetics experiments at high UTP (final concentrations 200 μM UTP and ATP, 10 μM GTP (no CTP), and labeling with 17.5 nM α-^{32}P-GTP). Amounts of each RNA length at each time are quantified by ^{32}P-UTP or ^{32}P-GTP incorporation. Efficient incorporation of the α-^{32}P label into the transcript is achieved by use of a low concentration (10 μM) of the corresponding unlabeled NTP.

Because RNAP escapes from this λP_R promoter in the conversion of 10-mer to 11-mer, all RNAs greater than 10-mer in length are defined as FL RNA (15). The transient accumulation of 12-mer and 13-mer may result from the reduction in rate constants for the subsequent steps caused by the coupling of translocation to disruption of σ^{70}-core RNAP contacts. Readthrough by misincorporation results in extension of the 16-mer RNA to the position of the next C in the transcript at +32, near the fragment end. Transcription occurs slowly near a fragment end, so this second pause is effectively a stop point.

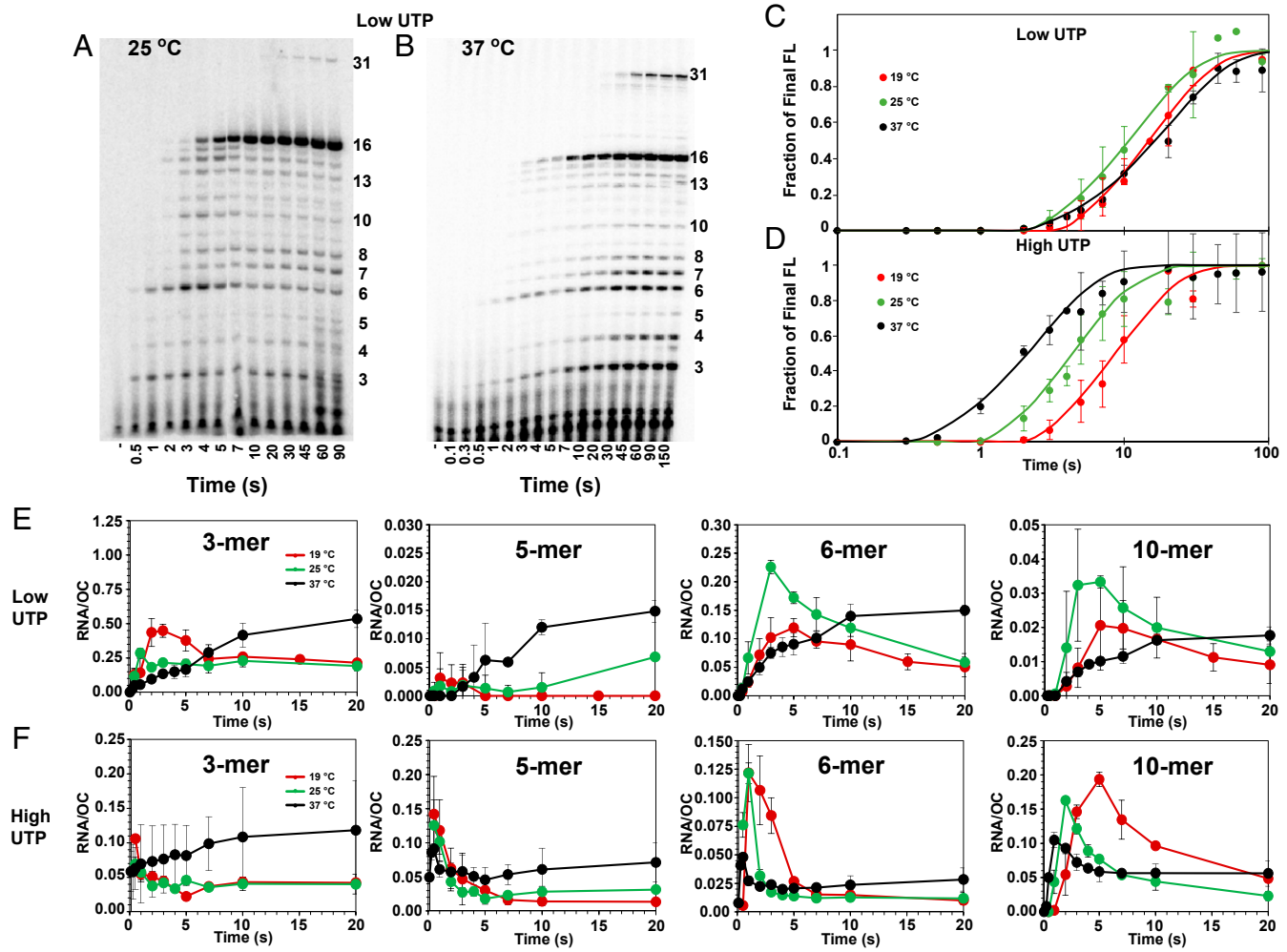

Fig. 2. Step-by-step kinetics of transcription initiation from λP_R promoter at different NTP concentrations and temperatures. (*Top Left*) PAGE separations of individual ^{32}P-labeled RNA bands (from 3-mer to 16-mer and 31-mer) observed as a function of time during productive and nonproductive initiation at 25 (*A*) and 37 °C (*B*). Lanes span the time range from 0.5 to 90 s or 0.1 to 150 s after adding NTPs and heparin to OC formed by premixing RNAP and λP_R-promoter DNA (*SI Appendix, Methods*). Gels shown are for the low-UTP condition: 200 μM ATP and GTP, 10 μM UTP, and 17.5 nM α-^{32}P-UTP. CTP is omitted, causing transcription to pause at a 16-mer RNA, before readthrough occurs to synthesize longer transcripts (15). Representative high-UTP (200 μM ATP and UTP, 10 μM GTP, and 17.5 nM α-^{32}P-GTP) gels at 25 and 37 °C are shown in *SI Appendix*, Fig. S1. (*Top Right*) Time courses (log scale) of synthesis of FL (>10-mer) RNA at 19 [red (15)], 25 (green), and 37 °C (black) at low UTP (*C*) and high UTP (*D*). (*Bottom*) Comparisons of linear time courses for representative short RNAs (3-mer, 5-mer, 6-mer, and 10-mer) synthesized by productive and nonproductive complexes at low UTP (*E*) and high UTP (*F*) at 19 [red (15)], 25 (green), and 37 °C (black). At each time point, the average amount of each RNA present (per OC) is shown with the estimated uncertainty.

FL RNA Synthesis. The kinetics of synthesis of FL RNA, determined by summing phosphorimager data for RNA species longer than 10-mer, are shown in Fig. 2 *C* and *D*. These compare time courses (log scale) of FL RNA synthesis for low-UTP and high-UTP conditions at 25 and 37 °C with previous results at 19 °C. Results are the averages of two to four independent experiments at each condition, including those in Fig. 2 *A* and *B* and *SI Appendix*, Fig. S1. In all cases, these kinetics are well described as a short lag phase, followed by a first order (single exponential) approach to a plateau value with rate constant k_{FL}, as observed previously at 19 °C (16). Values of the lag time and k_{FL} at high-UTP and low-UTP conditions at each temperature are given in *SI Appendix*, Table S3. At the plateau, 0.5 ± 0.15 FL RNA are synthesized per OC, demonstrating that ~50% of the λP_R OC population at all three temperatures are productive and capable of promoter escape, as previously observed at 19 and 37 °C (15, 16).

Arrhenius plots of ln k_{FL} versus 1/T are shown in *SI Appendix*, Fig. S2. At the high-UTP–low-GTP condition, ln k_{FL} decreases monotonically but not linearly with 1/T, indicating a positive Arrhenius activation energy that decreases with increasing temperature. At the low-UTP–high-GTP condition, all k_{FL} values are much smaller, despite a similar number of U and G bases incorporated into the FL transcript (3 U and 4 G by 11-mer formation, Fig. 1*A*). In addition, k_{FL} is larger at 25 °C than at 37 °C, corresponding to a negative activation energy in this temperature range (*SI Appendix*, Fig. S2) and indicating a change in the mechanism with increasing temperature. These observations can all be explained by an additional step early in the mechanism of FL RNA synthesis that is very significant at 37 °C but not at 19 °C and is favored at high-UTP concentration (see *Discussion*).

Transient Short RNA Intermediates in FL RNA Synthesis. Fig. 2 *E* and *F* show the time evolution of amounts of four different short RNAs (3-mer, 5-mer, 6-mer, and 10-mer) formed transiently in FL RNA synthesis by productive complexes at low-UTP and high-UTP conditions at 37 and 25 °C. Previously published results at 19 °C are shown for comparison. The results plotted are

averages obtained from the analysis of multiple gels, such as those in Fig. 2 *A* and *B*, and are normalized per OC.

At 25 °C, at both low UTP and high UTP, Fig. 2 *E* and *F* show that amounts of all four RNA species increase rapidly and then decrease in the first 10 s after NTP addition, consistent with previous observations at 19 °C and indicating significant transient intermediates on the pathway to productive synthesis (16). Each transient occurs earlier at 25 °C than at 19 °C at both NTP conditions, as expected since most reaction rates increase with increasing temperature. Each transient occurs earlier at high UTP than at low UTP at both temperatures, expected because UTP is a reactant in the first step of initial transcription (pppApU synthesis).

At 37 °C and low UTP, however, no significant transient population of any intermediate is observed in FL RNA synthesis. At 37 °C and high UTP, transient populations of some longer RNA intermediates (5-mer, 6-mer, 9-mer, and 10-mer) are detected, but no transients for shorter RNAs (3-mer and 4-mer) are observed, and transient peak amounts of longer RNAs are small by comparison to lower temperatures. These observations, and the slower synthesis of FL RNA at low UTP at 37 °C than at 25 °C (Fig. 2*C*), indicate that the population of λP_R OC at 37 °C, unlike at lower temperatures, is unable to productively bind the initiating NTP and synthesize pppApU without undergoing a conformational change. This conformational change is sufficiently unfavorable or slow to serve as a bottleneck and desynchronize subsequent steps of short RNA synthesis, so fewer transients are observed.

The stability of the λP_R OC is more than 30-fold greater at 37 °C than at 19 °C (27, 37). We previously proposed that the population distribution of λP_R OC also changed with temperature, shifting from the very stable 37 °C RP_O, with strong downstream interactions between RNAP DME and duplex DNA extending to +20, to a mixed population of RP_O and the I_3 intermediate OC (Fig. 1*C*) at lower temperature (27). If only I_3 and not RP_O can productively bind the two initiating NTP, then the differences in rates of FL RNA synthesis between 37 °C and lower temperatures are readily explained. In the *Discussion*, this proposal is incorporated into the initiation mechanism and used to analyze the kinetics of transient and FL RNA synthesis by productive complexes.

Discussion

Evidence for an OC Conformational Change Prior to NTP Binding at 37 °C but not at 19 °C. The mechanism previously used to interpret the kinetics of productive initiation at the λP_R promoter at 19 °C, including the appearance and disappearance of short RNA intermediates and the synthesis of FL RNA (16), is shown as Mechanism 1 in Fig. 3. This mechanism begins with ordered, reversible binding of the substrates (ATP [+1] and UTP [+2]) to the binary RNAP-promoter OC, followed by irreversible catalysis to synthesize the dinucleotide pppApU. No evidence was obtained for a conformational change in the OC prior to NTP binding at 19 °C (16).

Each subsequent step of initiation begins with reversible translocation. We previously deduced that most translocation steps in initiation are very unfavorable thermodynamically and rapidly reversible (16). Each translocation step in initiation requires the disruption of one downstream DNA–DNA base pair. In addition, translocation steps cause steric (6) and scrunching (31) stress as the RNA–DNA hybrid moves into the cleft, leading to disruption of RNAP-promoter contacts in many of these steps. Because translocation equilibrium constants for initiation steps are small, each step of the RNA–DNA hybrid extension up to the predicted point of escape is accurately quantified using a composite second-order rate constant k_i (the analog of an enzymatic k_{cat}/K_m; see ref. 16), as shown in Mechanism 1 (Fig. 3). Much higher NTP concentrations would be necessary to approach a maximum velocity condition and thereby separate contributions of the overall equilibrium constant for the reversible translocation and NTP binding steps (analog of $1/K_m$) from the rate constant of the irreversible catalytic step (k_{cat}). Fig. 3 shows the good fit of Mechanism 1 to the short RNA transients and FL RNA synthesis kinetics at 19 °C at both low- and high-UTP conditions.

Also shown in Fig. 3 are fits of productive initiation kinetic data to Mechanism 1 at 25 and 37 °C at low- and high-UTP conditions. At 25 °C, rate constants k_i obtained from these fits accurately reproduce the short RNA transients and FL RNA synthesis kinetics. However, it is clear from Fig. 3 that Mechanism 1 is not sufficient to describe the kinetics of productive initiation at 37 °C. To obtain an accurate fit to the 37 °C kinetic data requires the addition of an unfavorable reversible step at the beginning of the mechanism, prior to initial ATP binding (Fig. 3, Mechanism 2, step 1a). This step represents a conformational change, which we propose is the conversion of the very stable 37 °C OC (RP_O) to another OC conformation that we designate the initiating complex (IC). This step appears to be rapidly reversible and is characterized by the equilibrium constant K_{1a} (for $RP_O \rightarrow$ IC). All other steps of Mechanism 2 are the same as Mechanism 1. Fig. 3 also shows that use of Mechanism 2 to fit 19 and 25 °C datasets does not affect the quality of these fits and yields estimates of K_{1a} at these temperatures.

These fits predict that K_{1a} is extremely temperature dependent, greatly favoring RP_O at 37 °C ($K_{1a} \approx 0.01$; 99% RP_O) but favoring IC at 19 °C ($K_{1a} \approx 5.3$; more than 80% IC). A near-equimolar ratio of RP_O and IC is predicted at 25 °C ($K_{1a} \approx 0.70$; ~40% IC; ~60% RP_O). Good fits of 19 and 25 °C kinetic data to Mechanism 1 are obtained because a significant fraction of the OC population is initially in the IC conformation at these temperatures. The strong decrease in K_{1a} with increasing temperature indicates that the enthalpy change for the conversion of RP_O to IC is large in magnitude and negative; van 't Hoff analysis yields $\Delta H^o_{1a} = -60 \pm 20$ kcal/mol. The standard free energy change ΔG^o_{1a} for this conversion ranges from ~2.7 kcal at 37 °C to ~−1 kcal at 19 °C, and the corresponding entropy change ΔS^o_{1a} is −200 ± 60 eu. Conversion of RP_O to IC, therefore, shows near-complete enthalpy–entropy compensation, like many other protein processes.

Evidence that Only the I_3 Intermediate OC and not RP_O or I_2 Initiates Transcription from λP_R Promoter upon NTP Addition. Evidence exists for two open intermediates (I_2 and I_3) on the pathway to formation of the RP_O complex at the λP_R promoter (Fig. 1*C*). The thermodynamic, kinetic, and footprinting information available for these intermediates support the proposal that IC is I_3. I_2 is unstable with respect to I_3 and/or RP_O at higher temperatures and unstable with respect to CCs at lower temperatures (11, 17, 26, 27). Conversion of I_2 to I_3 involves the folding of 100 to 150 amino acid residues of RNAP DME (27) and is thought to strengthen contacts between the proximal downstream duplex, the β lobe, and the β' clamp (28). Conversion of I_3 to RP_O is thought to involve primarily an interaction of the downstream jaw and associated DME with the distal downstream duplex (+10 to +20), which serves to tighten the entire RNAP-promoter interface in the OC. The OC formed by the jaw deletion variant of RNAP and by downstream truncation variants of the promoter are thought to be models of I_3; equilibrium constants for forming these variant OC are one to two orders of magnitude smaller than the binding of wild-type (WT) RNAP to FL promoter DNA at 37 °C. Hydroxyl radical footprinting of the OC with the jaw deletion RNAP variant reveals that the entire RNAP-promoter interface in the OC is less protected and hence "looser" and more hydrated than in the WT RNAP OC (28).

From this body of previous research, the stable OC population was proposed to be an equilibrium mixture of I_3 and RP_O, with RP_O highly favored at 37 °C and I_3 increasing in significance at lower temperature (10, 28), but the details of this were not known. Here, we find that the stable OC population is an equilibrium mixture of RP_O and the IC initiation complex, with RP_O favored at 37 °C and IC favored below 25 °C, indicating that IC is I_3. In support of this, extrapolation of K_{1a} (Mechanism 2) to lower temperature, assuming a temperature-independent enthalpy change for $RP_O \rightarrow$ IC ($\Delta H^o_{1a} \approx -60$ kcal/mol), predicts that the IC:RP_O

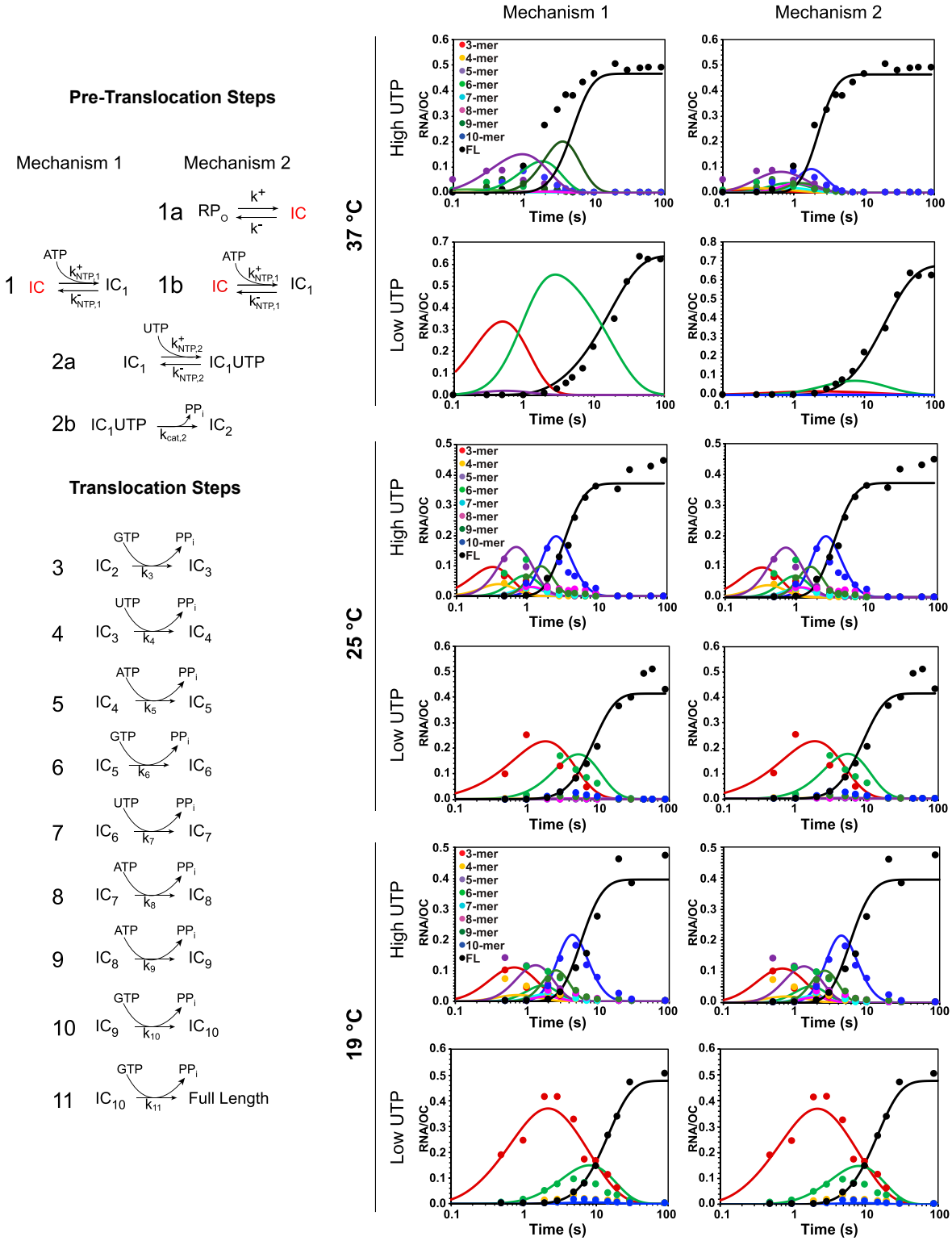

Fig. 3. Fits of initiation kinetic data to step-by-step mechanisms. (*Left*) Two mechanisms differing in initial (pretranslocation) steps are shown. Mechanism 1, previously shown to describe λP_R initiation data at 19 °C (15), is a minimal initiation mechanism for situations in which the stable OC is also the IC. Mechanism 2, proposed here to describe λP_R initiation data at 37 °C in which the stable OC is RP_O, includes an initial conformational change that converts RP_O to the IC that binds NTP and productively initiates as in Mechanism 1. (*Right*) Comparison of fits (solid curves) to Mechanisms 1 and 2 of all λP_R productive initiation data at 37, 25, and 19 °C for the two NTP conditions investigated (log time scale). Colors: 3-mer, red; 4-mer, yellow; 5-mer, purple; 6-mer, light green; 7-mer, light blue; 8-mer, pink; 9-mer, dark green; 10-mer, dark blue; and FL, black. The analyses of short RNA time courses (e.g., Fig. 2 *E* and *F*) to obtain the transients in FL RNA synthesis plotted here (points) are shown in *SI Appendix*, Figs. S3–S6. Rate constants k_i, determined from these fits to Mechanism 2 at each temperature, are given in *SI Appendix*, Table S4.

population distribution for λP_R at 10 °C, before NTP addition, is ~99% IC and only 1% RP_O. At 10 °C, Gries et al. (38) determined MnO_4^- footprints of both strands of the open region in the stable λP_R OC, now identified as the IC initiation complex. In addition, salt upshifts were used to rapidly destabilize the 10 °C λP_R OC and obtain a burst of I_2, the least stable open intermediate, for MnO_4^- footprinting. Hence, the 10 °C λP_R OC population, identified in the current research as 99% IC, is more stable and hence more advanced than I_2 at 10 °C and therefore must be I_3.

Kinetic–Mechanistic Evidence for Sequential Disruption of RNAP-Strand Contacts and Bubble Collapse in the Steps of Initiation. Fig. 4 (also *SI Appendix*, Table S4) compares rate constants k_i for each step of incorporation of NMP into the RNA–DNA hybrid at 25 and 37 °C with 19 °C values. All are calculated using Mechanism 2 (Fig. 3); the 19 °C values are not significantly different from those obtained previously using Mechanism 1 (16). Steps of initiation that involve translocation show the same pattern of large and small k_i values at all temperatures investigated. Three distinct regions of small k_i are observed in Fig. 4. These correspond to 1) synthesis of 4-mer and 5-mer; 2) synthesis of 7-mer, 8-mer, and 9-mer; and 3) synthesis of 11-mer and are separated by single steps, with larger k_i for synthesis of 3-mer, 6-mer, and 10-mer. In initiation, in which translocation is unfavorable because of steric and scrunching stress, k_i is interpretable (to a good approximation) as the product of the equilibrium constants for translocation and NTP binding and the catalytic rate constant k_{cat} (16).

To transition from initiation to elongation, the specific contacts between RNAP and promoter DNA that were essential to form and stabilize the OC must be broken. Previously, we interpreted the pattern of 19 °C k_i values in terms of the serial disruption of these promoter contacts. In this interpretation, differences in k_i values arise from differences in the equilibrium constant for translocation at each nucleotide addition step, $K_{tr,i}$. The very similar patterns of small and large k_i values observed in Fig. 4 at 37, 25, and 19 °C indicate that, at all three temperatures, interactions of RNAP with the discriminator strands (indicated as region a in Fig. 4) are broken in translocation preceding synthesis of 4-mer and 5-mer. Strong interactions of RNAP with the strands of the −10 region (region b in Fig. 4) are broken in translocation preceding synthesis of 7-mer, 8-mer, and 9-mer, and interactions of RNAP with the −35 and upstream regions (region c in Fig. 4) are disrupted in translocation prior to synthesis of an 11-mer.

Very different effects of temperature on k_i values for different translocation steps of initiation are observed in Fig. 4. For early (3-mer, 4-mer) and late (10-mer, 11-mer) steps, k_i values increase strongly with increasing temperature. For mid-initiation steps (5-mer, 6-mer, 7-mer, 8-mer), k_i values increase more modestly with increasing temperature. Notably, rate constant k_9 for 9-mer decreases with increasing temperature. Analysis of these temperature dependences yields Arrhenius activation energies $E_{act,i}$ (Fig. 4 and *SI Appendix*, Table S5), which vary by 30 kcal from +26 to −4 kcal.

$E_{act,2}$ for incorporation of UTP into pppApU, a step that does not involve translocation stress, is ~9 kcal, similar to that reported previously for steps of elongation by *E. coli* RNAP [10 to 13 kcal (39)]. $E_{act,3}$ and $E_{act,4}$ for 3-mer and 4-mer are significantly larger (~26 kcal), while E_{act} values for the next five steps are quite small (~6 kcal for synthesis of 5-mer, 6-mer, 7-mer, and 8-mer RNA and ~−4 kcal for 9-mer). Contacts of RNAP with the strands of the upstream bubble (positions -1 to -11 relative to the +1 TSS) are proposed to be disrupted in many of these steps (16). An interpretation of k_i and $E_{act,i}$ values in terms of changes in base stacking in these steps is given in the section *Identifying Contributions of Downstream DNA Melting and of Base Stacking and Duplex Formation of the Upstream Bubble to the Kinetics of Initiation Steps*. $E_{act,10}$ and $E_{act,11}$ are larger than the previous E_{act} values, though not as large as $E_{act,3}$ and $E_{act,4}$.

From rate constants k_i and activation energies $E_{act,i}$, the quasithermodynamic quantities $\Delta G_i^{o\ddagger}$, $\Delta H_i^{o\ddagger}$, and $\Delta S_i^{o\ddagger}$, for each step, can be determined if the hypothetical maximum second-order rate constant k_{max} for this process (at $\Delta G_i^{o\ddagger} = 0$) and its temperature dependence are known. These $\Delta G_i^{o\ddagger}$, $\Delta H_i^{o\ddagger}$, and $\Delta S_i^{o\ddagger}$ are for

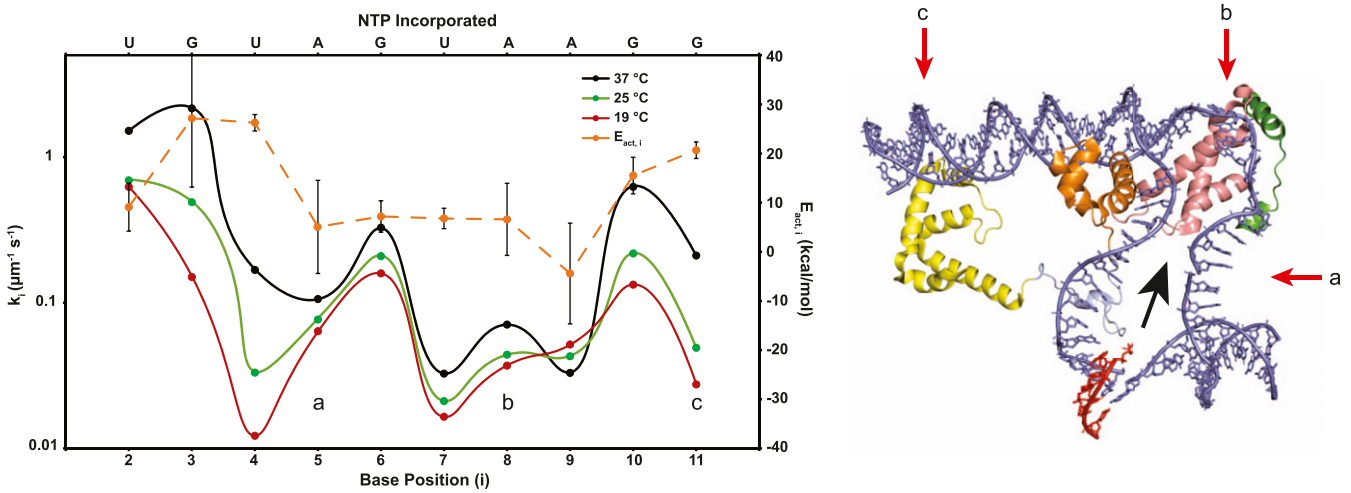

Fig. 4. (*Left*) Comparison of rate constants and activation energies for individual steps of initiation. Composite rate constants k_i (left axis; micromolar^{-1} · seconds^{-1}) for each step (i) of NMP incorporation and hybrid extension before the escape of RNAP are plotted on a log scale for the λP_R promoter at 19 [red (15)], 25 (green), and 37 °C (black). At each temperature, differences in k_i values are interpreted as differences in the equilibrium constant $K_{tr,I}$ for translocation that occurs before NTP binding and catalysis in steps 3 to 11. Three regions of small k_i (and therefore small $K_{tr,\ i}$) values, observed at all temperatures, are labeled a, b, and c for comparison with the framework ITC structure (*Right*). Arrhenius activation energies ($E_{act,\ i}$, orange, and right axis) of initial transcription steps, determined from the temperature dependences of the individual k_i (*SI Appendix*, Fig. S7), are also shown. (*Right*) Structural representation of an ITC. This ITC framework structure (adapted from 4YLP) employed a promoter heteroduplex in the region of the initiation bubble and a 5-mer RNA hybridized to the template strand (RNA in red and promoter DNA in blue). Relevant regions of σ^{70} include $\sigma_{1.2}$ (green), σ_2 (pink), σ_3 (orange), $\sigma_{3.2}$ (light blue), and σ_4 (yellow). Letters a, b, and c indicate the discriminator and −10 regions of the bubble strands and the −35 duplex, respectively. The expected direction of translocation of the hybrid into the RNAP cleft in initiation is indicated by the black arrow. Translocation is proposed to disrupt RNAP-promoter contacts with regions a, b, and c in the steps of initiation with small rate constants (indicated by the corresponding letters on the k_i plot [*Left*]), resulting in stepwise bubble collapse.

conversion of the reactants in the i-th step (NTP, pretranslocated initiation complex) to the subsequent catalytic transition state. We assume that all steps have the same k_{max} and approximate it by the value for an orientation-corrected, diffusion-limited rate constant ($k_{max} \approx 10^3\ \mu M^{-1} \cdot s^{-1}$), neglecting the small temperature dependence of a diffusion-limited k_{max} in calculating $\Delta H_i^{o\ddagger}$ values (40). Although the uncertainty in the appropriate value of k_{max} is probably one order of magnitude, this is of no consequence for the following analysis (see also *SI Appendix*, Tables S5 and S6) as long as k_{max} has the same value for each step.

For $k_{max} \approx 10^3\ \mu M^{-1} \cdot s^{-1}$, $\Delta G_2^{o\ddagger}$ for incorporation of the initiating UTP into pppApU is ~4.3 kcal, and values of $\Delta G_i^{o\ddagger}$ for subsequent steps of initiation ($3 \le i \le 11$) are in the range ~5.1 to ~6.6 kcal (*SI Appendix*, Table S5). Values of $\Delta H_i^{o\ddagger}$ and $\Delta S_i^{o\ddagger}$ vary over much wider ranges (~30 kcal range in $\Delta H_i^{o\ddagger} = E_{act,i}$; ~100 eu range in $\Delta S_i^{o\ddagger}$) (*SI Appendix*, Table S5). For incorporation of the initiating UTP into pppApU (2-mer synthesis), $\Delta H_2^{o\ddagger}$ and $\Delta S_2^{o\ddagger}$ are modest (9 kcal and 16 eu). The values of $\Delta G_2^{o\ddagger}$, $\Delta H_2^{o\ddagger}$, and $\Delta S_2^{o\ddagger}$ include contributions from the thermodynamics of UTP binding, including stacking of UTP on ATP, and from the intrinsic activation quantities for the catalytic step, but do not include any contributions from translocation.

Values of $\Delta H_i^{o\ddagger}$ and $\Delta S_i^{o\ddagger}$ for subsequent steps involving translocation are very different from those of 2-mer synthesis. Values of $\Delta H_i^{o\ddagger}$ and $\Delta S_i^{o\ddagger}$ for 3-mer and 4-mer are much larger than for 2-mer, while values of $\Delta H_i^{o\ddagger}$ and $\Delta S_i^{o\ddagger}$ for 5-mer, 6-mer, 7-mer, and 8-mer are much smaller (*SI Appendix*, Table S5), and values of $\Delta H_9^{o\ddagger}$ and $\Delta S_9^{o\ddagger}$ for 9-mer are modestly negative. These steps involving translocation include those identified previously as ones in which contacts of the discriminator and −10 strands with RNAP are disrupted, freeing the initiation bubble strands. $\Delta H_i^{o\ddagger}$ and $\Delta S_i^{o\ddagger}$ for 10-mer and 11-mer are more comparable to 3-mer and 4-mer. Contacts that are disrupted in these steps are proposed to be with the duplex (−35 and upstream) and not with ssDNA. Hence, the unusual activation thermodynamics are confined to the steps that break RNAP contacts with the bubble strands.

Identifying Contributions of Downstream DNA Melting and of Base Stacking and Duplex Formation of the Upstream Bubble to the Kinetics of Initiation Steps. Disruption of base-stacking interactions in the melting of double-helical DNA to two separated strands is a major determinant of the melting enthalpy (41). Bases in ss nucleic acids are highly stacked in solution at 0 °C and unstack noncooperatively with increasing temperature. The enthalpy change for base unstacking in ssDNA is ~5 kcal · mol^{-1}, and the enthalpy of duplex melting is predicted to vary from ~5 kcal · $(mol\ base\ pair)^{-1}$ under conditions in which the bases in the separated strands are fully stacked to ~15 kcal · $(mol\ base\ pair)^{-1}$ under conditions in which the bases in the separated strands are fully unstacked (41).

Steps synthesizing 3-mer and 4-mer, the first two steps of initiation that begin with translocation and melting of one base pair at the downstream end of the initiation bubble, exhibit activation energies and enthalpies that are ~17 kcal larger than for the step synthesizing 2-mer, which at the λP_R promoter requires neither translocation nor base pair melting. Melting of one base pair can account for much of the 17 kcal differences between $\Delta H_3^{o\ddagger}$ or $\Delta H_4^{o\ddagger}$ versus $\Delta H_2^{o\ddagger}$, depending on the extent to which the bases after melting are unstacked.

Since subsequent steps of initiation also involve translocation and melting of one downstream DNA base pair, how can the very small (and in one case negative)$\Delta H_i^{o\ddagger}$values for the five subsequent steps of initiation (5-mer to 9-mer synthesis) be explained? *SI Appendix*, Table S5 shows that values of $\Delta H_i^{o\ddagger}$ for 5-mer to 8-mer synthesis are ~20 kcal less positive, and $\Delta H_i^{o\ddagger}$ for 9-mer synthesis is ~30 kcal less positive than for 3-mer and 4-mer synthesis.

Previously, to explain the pattern of small and large rate constants of these steps, we proposed that contacts of RNAP with the discriminator and −10 regions of the bubble strands are disrupted in a stepwise manner, beginning at the downstream end of the template and/or nontemplate discriminator strands, as the hybrid lengthens to a 9-mer. Here, to explain the unusual values of $\Delta H_i^{o\ddagger}$ for 5-mer to 9-mer synthesis, we propose that the substantial stacking of bases in these strands accompanies the release of contacts with RNAP. A comparison of permanganate reactivities of thymines in the open region of the stable OC I_3 and the unstable I_2 revealed that most thymines in I_3 are significantly more reactive and hence more exposed than in I_2 (38). To explain this, we proposed that bases in the open region of I_3 are much more unstacked than in I_2 because of tighter binding of the strand backbones in the open region of I_3 (38). Precedent for base unstacking in formation of a protein–ssDNA complex, in which the DNA backbone is strongly bound, is provided by the very stable SSB–ssDNA complex (42). Hence, base stacking is expected to accompany the disruption of contacts between RNAP and the open strands of the initiation bubble in steps of initiation involving translocation. The 20 to 30 kcal reductions in $\Delta H_i^{o\ddagger}$ for 5-mer to 9-mer synthesis, compared to 3-mer and 4-mer synthesis, are consistent with the stacking of four bases in each step of synthesis of 5-mer, 6-mer, 7-mer, and 8-mer and stacking of six bases in synthesis of 9-mer (*SI Appendix*, Table S6).

We expected to observe a large negative contribution to $\Delta H_i^{o\ddagger}$ from duplex formation by the bubble strands in one or more late steps of initiation. Formation of an 11 base pair duplex is predicted to contribute at least −50 kcal · mol^{-1} to $\Delta H_i^{o\ddagger}$ if those strands are already stacked and as much as −150 kcal · mol^{-1} if they are initially unstacked. From the analysis in *SI Appendix*, Table S5, the only step that could include a negative enthalpy term of this magnitude is 9-mer formation, in which we identify a −30kcal contribution that could be from duplex formation from fully stacked strands. The smaller magnitude of this contribution (−30 versus −50 kcal · mol^{-1}) could result from the need to break enthalpically, favorable interactions of the −7 and −11 bases on the nontemplate strand with aromatic residues in the base-binding pockets of sigma region 2 (29).

Alternatively, base pair formation may occur incrementally as the hybrid extends from a 5-mer to 9-mer. Base pair formation (including base stacking) in these steps would also explain their small activation enthalpies. Base pair formation would explain the finding (in the preceding paragraph; see also *SI Appendix*, Table S6) that base stacking increases in increments of four or six bases (i.e., two or three base pairs) in these steps. Base pair formation can also explain the offset between the first step with a small rate constant (4-mer synthesis, accompanied by disruption of some RNAP–discriminator strand interactions) and the first step with a small activation energy (5-mer synthesis, accompanied by formation of four base-stacking interactions or two base pairs). This offset would not be expected for ss stacking interactions but is explained if RNAP interactions with the downstream end of one discriminator strand are disrupted in 4-mer synthesis, while interactions with this region of the other strand are disrupted in 5-mer synthesis, allowing base pairing. A structural interpretation of activation enthalpies (*SI Appendix*, Table S5), in terms of step-by-step base pairing as RNAP-strand contacts are disrupted in initiation, is given in *SI Appendix*, Table S6. Because structural studies of initiation complexes to date have used heteroduplexes with an open initiation bubble, they provide no information about the extent of pairing of the bases that accompanies the synthesis of 5-mer or longer RNA in a productive initiation complex.

Conclusions

We find that the λP_R initiation complex is the intermediate OC I_3 (Fig. 1) and not the very stable RP_O. Initiation at 37 °C, in which the λP_R OC is predominantly RP_O, requires an initial

BIOCHEMISTRY

conformational change to form I_3 before productive binding of both initiating NTPs. We also find that the disruption of RNAP contacts with the strands of the initiation bubble and bubble collapse occur stepwise in initiation, prior to disruption of RNAP contacts with the upstream duplex and escape of RNAP from the promoter. At a minimum, stepwise bubble collapse involves stepwise stacking of ss bases and may also involve stepwise base pairing. The activation thermodynamics provide no evidence that duplex formation by the bubble strands is delayed until the RNAP escape point (11-mer RNA formation), when interactions with the −35 region upstream duplex are proposed to be disrupted. Instead, the activation thermodynamics are consistent with duplex formation in one or more earlier steps, in which contacts of the bubble strands with the discriminator and −10 region are disrupted. Analogous quantitative studies of initiation kinetics and mechanism at other promoters and for λP_R with different discriminator lengths and ITR are needed to characterize the relationship between promoter identity, initiation kinetics and mechanism, and the regulatory possibilities therein.

Materials and Methods

Details about reagents (buffers, enzymes, and DNA), initiation kinetic assays (single round in synthesis of FL RNA), and analysis of amounts of transient short RNAs from productive complexes and of stalled and released short RNA from nonproductive complexes are described in *SI Appendix*, with references to previous publications. Briefly, the λP_R OC is preformed by incubation at the experimental temperature (25 or 37 °C) for 1 h. Preformed OC and initiation solution containing NTPs and heparin are mixed 1:1 at time 0 using a Kintek Corp Rapid Quench Flow, and quenched with 8 M urea and 15 mM EDTA at the times indicated. RNA products are visualized and quantified using PAGE, followed by phosphorimager analysis of incorporated α-32P-NTPs, as described previously (15). Fits were obtained using Kintek Explorer.

Data Availability. All study data are included in the article and/or *SI Appendix*.

ACKNOWLEDGMENTS. D.M.P. was supported by NIH Biotechnology Traineeship NIH Grant 5 T32 GM008349 and K.L.H. by NIH National Research Service Award postdoctoral fellowship NIH Grant GM 122303. We gratefully acknowledge the very helpful comments of the editor and reviewers and the support for this research from the abovementioned fellowships, University of Wisconsin–Madison, and NIH Grant GM R35-118100 (M.T.R.).

1. R. M. Saecker, M. T. Record Jr, P. L. Dehaseth, Mechanism of bacterial transcription initiation: RNA polymerase – Promoter binding, isomerization to initiation-competent open complexes, and initiation of RNA synthesis. *J. Mol. Biol.* **412**, 754–771 (2011).
2. S. P. Haugen, W. Ross, M. Manrique, R. L. Gourse, Fine structure of the promoter-sigma region 1.2 interaction. *Proc. Natl. Acad. Sci. U.S.A.* **105**, 3292–3297 (2008).
3. C. J. Dorman, Co-operative roles for DNA supercoiling and nucleoid-associated proteins in the regulation of bacterial transcription. *Biochem. Soc. Trans.* **41**, 542–547 (2013).
4. J. Chen, H. Boyaci, E. A. Campbell, Diverse and unified mechanisms of transcription initiation in bacteria. *Nat. Rev. Microbiol.* **19**, 95–109 (2021).
5. J. Chen *et al*., Stepwise promoter melting by bacterial RNA polymerase. *Mol. Cell* **78**, 275–288.e6 (2020).
6. Y. Zuo, T. A. Steitz, Crystal structures of the *E. coli* transcription initiation complexes with a complete bubble. *Mol. Cell* **58**, 534–540 (2015).
7. L. Li, V. Molodtsov, W. Lin, R. H. Ebright, Y. Zhang, RNA extension drives a stepwise displacement of an initiation-factor structural module in initial transcription. *Proc. Natl. Acad. Sci. U.S.A.* **117**, 5801–5809 (2020).
8. Y. Shin *et al*., Structural basis of ribosomal RNA transcription regulation. *Nat. Commun.* **12**, 528 (2021).
9. R. Glyde *et al*., Structures of bacterial RNA polymerase complexes reveal the mechanism of DNA loading and transcription initiation. *Mol. Cell* **70**, 1111–1120.e3 (2018).
10. E. F. Ruff *et al*., *E. coli* polymerase determinants of open complex lifetime and structure. *J. Mol. Biol.* **427**, 2435–2450 (2015).
11. E. F. Ruff, M. T. Record Jr, I. Artsimovitch, Initial events in bacterial transcription initiation. *Biomolecules* **5**, 1035–1062 (2015).
12. J. Ko, T. Heyduk, Kinetics of promoter escape by bacterial RNA polymerase: Effects of promoter contacts and transcription bubble collapse. *Biochem. J.* **463**, 135–144 (2014).
13. D. Duchi *et al*., RNA polymerase pausing during initial transcription. *Mol. Cell* **63**, 939–950 (2016).
14. E. A. Hubin *et al*., Structure and function of the mycobacterial transcription initiation complex with the essential regulator RbpA. *eLife* **6**, e22520 (2017).
15. K. L. Henderson *et al*., Mechanism of transcription initiation and promoter escape by *E. coli* RNA polymerase. *Proc. Natl. Acad. Sci. U.S.A.* **114**, E3032–E3040 (2017).
16. K. L. Henderson *et al*., RNA polymerase: Step-by-step kinetics and mechanism of transcription initiation. *Biochemistry* **58**, 2339–2352 (2019).
17. R. Sreenivasan *et al*., Fluorescence-detected conformational changes in duplex DNA in open complex formation by E. coli RNA polymerase: Upstream wrapping and downstream bending precede clamp opening and insertion of the downstream duplex. *Biochemistry* **59**, 1565–1581 (2020).
18. D. Jensen, A. R. Manzano, J. Rammohan, C. L. Stallings, E. A. Galburt, CarD and RbpA modify the kinetics of initial transcription and slow promoter escape of the *Mycobacterium tuberculosis* RNA polymerase. *Nucleic Acids Res.* **47**, 6685–6698 (2019).
19. E. Lerner *et al*., Backtracked and paused transcription initiation intermediate of *Escherichia coli* RNA polymerase. *Proc. Natl. Acad. Sci. U.S.A.* **113**, E6562–E6571 (2016).
20. E. Heyduk, T. Heyduk, DNA template sequence control of bacterial RNA polymerase escape from the promoter. *Nucleic Acids Res.* **46**, 4469–4486 (2018).
21. J. T. Winkelman *et al*., XACT-seq comprehensively defines the promoter-position and promoter-sequence determinants for initial-transcription pausing. *Mol. Cell* **79**, 797–811.e8 (2019).
22. L. Han *et al*., Development of a novel strategy for robust synthetic bacterial promoters based on a stepwise evolution targeting the spacer region of the core promoter in *Bacillus subtilis*. *Microb. Cell Fact.* **18**, 96 (2019).
23. L. Yu *et al*., The mechanism of variability in transcription start site selection. *eLife* **6**, e32038 (2017).
24. E. Heyduk, T. Heyduk, Next generation sequencing-based parallel analysis of melting kinetics of 4096 variants of a bacterial promoter. *Biochemistry* **53**, 282–292 (2014).
25. W. S. Kontur, R. M. Saecker, C. A. Davis, M. W. Capp, M. T. Record Jr, Solute probes of conformational changes in open complex (RPo) formation by Escherichia coli RNA polymerase at the lambdaPR promoter: Evidence for unmasking of the active site in the isomerization step and for large-scale coupled folding in the subsequent conversion to RPo. *Biochemistry* **45**, 2161–2177 (2006).
26. W. S. Kontur, M. W. Capp, T. J. Gries, R. M. Saecker, M. T. J. Record Jr, Probing DNA binding, DNA opening, and assembly of a downstream clamp/jaw in *Escherichia coli* RNA polymerase-lambdaP(R) promoter complexes using salt and the physiological anion glutamate. *Biochemistry* **49**, 4361–4373 (2010).
27. W. S. Kontur, R. M. Saecker, M. W. Capp, M. T. J. Record Jr, Late steps in the formation of *E. coli* RNA polymerase-λ P_R promoter open complexes: Characterization of conformational changes by rapid [perturbant] upshift experiments. *J. Mol. Biol.* **376**, 1034–1047 (2008).
28. A. Drennan *et al*., Key roles of the downstream mobile jaw of *Escherichia coli* RNA polymerase in transcription initiation. *Biochemistry* **51**, 9447–9459 (2012).
29. Y. Zhang *et al*., Structural basis of transcription initiation. *Science* **338**, 1076–1080 (2012).
30. A. Revyakin, R. H. Ebright, T. R. Strick, Promoter unwinding and promoter clearance by RNA polymerase: Detection by single-molecule DNA nanomanipulation. *Proc. Natl. Acad. Sci. U.S.A.* **101**, 4776–4780 (2004).
31. A. N. Kapanidis *et al*., Initial transcription by RNA polymerase proceeds through a DNA-scrunching mechanism. *Science* **314**, 1144–1147 (2006).
32. A. Revyakin, C. Liu, R. H. Ebright, T. R. Strick, Abortive initiation and productive initiation by RNA polymerase involve DNA scrunching. *Science* **314**, 1139–1143 (2006).
33. J. T. Winkelman *et al*., Crosslink mapping at amino acid-base resolution reveals the path of scrunched DNA in initial transcribing complexes. *Mol. Cell* **59**, 768–780 (2015).
34. A. Feklistov, S. A. Darst, Structural basis for promoter-10 element recognition by the bacterial RNA polymerase σ subunit. *Cell* **147**, 1257–1269 (2011).
35. T. M. Stackhouse, A. P. Telesnitsky, C. F. Meares, Release of the sigma subunit from *Escherichia coli* RNA polymerase transcription complexes is dependent on the promoter sequence. *Biochemistry* **28**, 7781–7788 (1989).
36. H. R. Koh *et al*., Correlating transcription initiation and conformational changes by a single-subunit RNA polymerase with near base-pair resolution. *Mol. Cell* **70**, 695–706.e5 (2018).
37. R. M. Saecker *et al*., Kinetic studies and structural models of the association of *E. coli* sigma(70) RNA polymerase with the lambdaP(R) promoter: Large scale conformational changes in forming the kinetically significant intermediates. *J. Mol. Biol.* **319**, 649–671 (2002).
38. T. J. Gries, W. S. Kontur, M. W. Capp, R. M. Saecker, M. T. Record Jr, One-step DNA melting in the RNA polymerase cleft opens the initiation bubble to form an unstable open complex. *Proc. Natl. Acad. Sci. U.S.A.* **107**, 10418–10423 (2010).
39. Y. X. Mejia, H. Mao, N. R. Forde, C. Bustamante, Thermal probing of *E. coli* RNA polymerase off-pathway mechanisms. *J. Mol. Biol.* **382**, 628–637 (2008).
40. O. G. Berg, P. H. von Hippel, Diffusion-controlled macromolecular interactions. *Annu. Rev. Biophys. Biophys. Chem.* **14**, 131–160 (1985).
41. J. A. Holbrook, M. W. Capp, R. M. Saecker, M. T. Record Jr, Enthalpy and heat capacity changes for formation of an oligomeric DNA duplex: Interpretation in terms of coupled processes of formation and association of single-stranded helices. *Biochemistry* **38**, 8409–8422 (1999).
42. A. G. Kozlov, T. M. Lohman, Adenine base unstacking dominates the observed enthalpy and heat capacity changes for the *Escherichia coli* SSB tetramer binding to single-stranded oligoadenylates. *Biochemistry* **38**, 7388–7397 (1999).